



Investigation of interactions in the mechanically activated α -Fe₂O₃/ Li₂CO₃ reagents by thermal analysis

Evgeniy V. Nikolaev¹ · Elena N. Lysenko¹ · Anatoliy P. Surzhikov¹ · Vladimir D. Elkin¹

Received: 3 November 2021 / Accepted: 17 May 2022 / Published online: 10 June 2022
© Akadémiai Kiadó, Budapest, Hungary 2022

Abstract

The paper addresses the study of the effect of different milling modes on the reactivity of the initial α -Fe₂O₃ and Li₂CO₃ powders by thermogravimetry and differential scanning calorimetry to obtain lithium ferrite of Li_{0.5}Fe_{2.5}O₄ chemical composition. The formation of the magnetic phase of ferrite was monitored by thermogravimetric analysis in a magnetic field. The powder mixture was mechanically activated in air at different processing time and vial rotation speed using a planetary mill. It was found that the reactivity of the initial reagents depends on milling energy intensity. A varied milling mode changes the pattern of the interaction between reagents, and therefore a temperature range, the number of stages and the rate of lithium ferrite formation. In these conditions, an increased vial rotation speed during milling makes a more significant contribution to the change in the powder reactivity as compared to longer milling time.

Keywords Lithium ferrite · Li_{0.5}Fe_{2.5}O₄ · Mechanical activation · Solid-state synthesis · Thermogravimetry · DSC

Introduction

Solid-phase processes in ferrites initiated by mechanical action have been intensively studied over the past 30 years [1–5]. The reason for this is high potential of mechanical treatment in production of ferrite materials aimed at creating a more economically profitable technological process.

Thus, mechanical treatment was used to produce ferrites based on spinel MFe₂O₄ (M = Li⁺, Ni²⁺, Cu²⁺, Co²⁺, Zn²⁺, Mg²⁺) [6–10], ferrites with a hexagonal structure [11–14] and garnets [15, 16], etc.

Most of the studies on mechanical activation of ferrites were performed using planetary ball mills with a vertical rotation axis, for example, "Fritsch", "Retsch" or "Spex" [17–21]. The AGO-2 planetary ball mill is also widely used

[22, 23]. These devices are characterized by the main parameter, the rotation speed of the vials, which determines the milling mode. However, the efficiency of mechanical treatment depends not only on the milling mode, but also on the material and diameter of the balls and vials, and on the powder-to-balls mass ratio [24, 25]. One can notice that the milling intensity can be increased by increasing the rotation speed and mass of balls. However, an excessive increase in the mass of balls and improperly selected material of balls and vials can cause contamination of the processed powders and wear of the grinding media.

As shown in [26–30], the reaction of lithium ferrite formation depends on milling conditions. It should be noted that ferrite is not formed during milling of a mixture of reagents based on oxides and carbonates. During milling, reagents are only mechanically activated, which accelerates chemical processes in further ferrite synthesis.

For example, Berbenni et al. [26] showed that mechanical activation of iron oxide and lithium carbonate in a high-energy vibration mill for 2 or 5 h decreases the temperature of the synthesis reaction of lithium ferrite Li_{0.5}Fe_{2.5}O₄ by 200 °C. In this case, the microstructure of ferrite formed from milled powders is characterized by the α and β phase, while ferrite obtained from the initial powders contains only the α phase. In [27], Widatallah et al. also reported the formation of lithium ferrite containing both the α and β phase at

✉ Evgeniy V. Nikolaev
nikolaev0712@tpu.ru

Elena N. Lysenko
lysenkoen@tpu.ru

Anatoliy P. Surzhikov
surzhikov@tpu.ru

Vladimir D. Elkin
vde2@tpu.ru

¹ Tomsk Polytechnic University, Lenin Avenue 30, Tomsk, Russia 634050

lower temperatures in the case of using α -Fe₂O₃ and Li₂CO₃ powder reagents activated at 200 rpm for 50–135 h. Kavanlooe et al. used a planetary mill with a rotation speed of 450 rpm and a milling time of 40 h to obtain lithium-zinc-titanium ferrite [28]. Virtually all the studies that investigate lithium ferrite production employed a low vial rotation speed and, therefore, a long milling time.

In [29], it was found that 1-h mechanical activation of the initial powders at vial rotation speeds exceeding 2000 rpm significantly changes their reactivity. This makes it possible to considerably reduce the temperature and duration of synthesis, especially when using substituted ferrites with a complex chemical composition. In [30], the effect of mechanical activation on the reactivity and the temperature range of the reaction of lithium ferrite synthesis was shown separately for powders and mixtures based on them.

Wide variation in the milling mode available with modern ball mills and a limited number of publications in this area do not allow unambiguous conclusion about a more efficient milling mode for ferrite production.

The aim of this study is to investigate the effect of different vial rotation speeds of milling modes on the reactivity of the initial α -Fe₂O₃ and Li₂CO₃ powders using thermogravimetry (TG), differential scanning calorimetry (DSC) and laser diffraction analysis.

Experimental

The initial powders based on iron oxide and lithium carbonate (99%, Reahim Co., Russia) were used for lithium ferrite production. The α -Fe₂O₃ and Li₂CO₃ powders were preliminarily dried in the furnace at 200 °C and weighed in a molar ratio of 5:1.

An AGO-2 planetary ball mill (Novic, Russia), which is characterized by two grinding 150 mL steel vials and water-cooling of the outer sides of the vials, was used for mechanical activation. This ball mill allows three vial rotation speeds of 1290, 1820 and 2220 rpm that correspond to centrifugal acceleration of 300, 600 and 1000 m s⁻², respectively. The study employed 1290 and 2220 rpm modes, and the milling time was up to 120 min. The 6-mm steel balls and 20 g powder were used for milling. The powder-to-balls mass ratio was 1:10.

The particle size distribution of milled powder mixtures was analyzed by laser diffraction using a Fritsch Analysette 22 MicroTec Plus analyzer.

The ferrite synthesis reaction was studied using TG/DSC and mass spectrometric analysis by heating the 5 mg powder mixture to 800 °C in the furnace of a Netzsch STA 449C Jupiter thermal analyzer coupled to a QMS 403C Aélös mass spectrometer. Thermal analyzers like these are widely used in the analysis of ferrite materials [31–33].

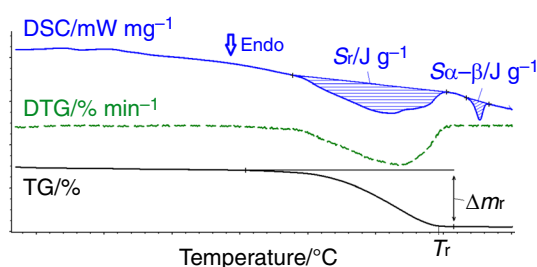


Fig. 1 TG, DSC and DTG curves for sample synthesized in thermal analyzer

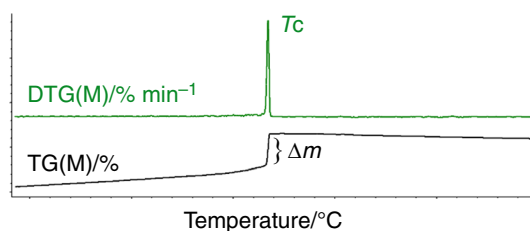


Fig. 2 TG and DTG curves for magnetic sample using magnetic field

Figure 1 illustrates typical behavior of the TG, DSC and derivative thermogravimetric (DTG) curves during heating of the powder mixture in accordance with the $\text{Li}_2\text{CO}_3 + 5\text{Fe}_2\text{O}_3 \rightarrow 4\text{Li}_{0.5}\text{Fe}_{2.5}\text{O}_4 + \text{CO}_2\uparrow$ reaction. In Fig. 1, S_r and $S_{\alpha-\beta}$ on the DSC curve indicate the area of the endothermic peak corresponding to the interaction between the reagents and the area of the peak during transition from α (order) to β (disorder) in the $\text{Li}_{0.5}\text{Fe}_{2.5}\text{O}_4$ ferrite phase formed during heating, respectively; Δm_r and T_r on the TG curve are the mass change due to CO₂ release and the final reaction temperature, respectively. The reaction temperature range depends on several factors, including the heating rate during thermal analysis [34] and the activity of the initial reagents [23]. In this study, all the samples were investigated at heating rate of 5 °C min⁻¹.

As was shown earlier in [23, 30], lithium ferrite is formed during heating in thermal analysis. The amount of the formed ferrite phase can be found either by the analysis of $S_{\alpha-\beta}$ on the DSC curve during heating or the reverse transition during cooling, as well as by measuring the Curie temperature at the cooling stage from 800 °C to room temperature [30, 35]. In the latter case, two permanent magnets were used, which were connected to the furnace of the thermal analyzer at the beginning of the cooling stage. Figure 2 shows a typical pattern of the TG(M) and DTG(M) curves for measurements in a magnetic field using the Netzsch STA 449C Jupiter analyzer. In this case, the mass change (Δm) depends only on the interaction of the sample with the magnetic field, and not on its probable chemical changes.

However, in all experiments, corrections were made to the experimental curves by measuring the TG curves taken on an empty crucible.

Results and discussion

The particle size distributions of the Fe₂O₃ and Li₂CO₃ initial reagents were investigated in [29].

In this study, the particle size distribution of Fe₂O₃/Li₂CO₃ powder mixtures was analyzed. From [29], Fe₂O₃ and Li₂CO₃ powders are characterized by bimodal distribution in 0.2–3/3–40 μ m and 3–50/50–300 μ m ranges with the average particle size of 12.1 and 47.2 μ m, respectively. The SEM images of Fe₂O₃ and Li₂CO₃ powders were also shown in [29].

Figure 3 shows the result of the analysis of non-activated powders (Fig. 3a), and for powders activated at 1290 rpm (Fig. 3b) and 2220 rpm (Fig. 3c) for 120 min. Table 1 presents the main characteristics obtained from the analysis. All the samples exhibit a bimodal particle size distribution in the range of 0.2–5 μ m and 5–50 μ m. One can notice that the distribution for mixtures has a behavior similar to the distribution of the Fe₂O₃ as the concentration of iron oxide in total mixture was 91.5 mass%. The average particle size for the non-activated powder mixture is 16.7 μ m, while for those activated at 1290 rpm and 2220 rpm, it attains 12.6 and 11.6 μ m, respectively. No significant particle size reduction to submicron size can be observed. However, the content of fine particles significantly increases up to 5 μ m in the activated powders. Ultrasound employed in laser diffraction did not significantly change the analysis results.

In this study, thermal analysis was carried out for samples containing initial powders and powders that were preliminarily mechanically activated with milling time from 5 to 120 min. Figures 4–6 show thermal analysis results for non-activated (0 rpm) and activated at 1290 and 2220 rpm for 120 min samples.

The analysis results for the samples based on non-activated powders are very similar to the results previously obtained by thermal analysis of the Fe₂O₃/Li₂CO₃ mixture and presented in [30]. Since the peak areas on the DSC curve for these samples depend on the bulk density of the powder in the crucible, which is very difficult to maintain during the experiments, the S_r values obtained differ somewhat from the values presented in [30]. As can be seen from Fig. 4a, b, the reaction of interaction between the non-activated reagents is followed by a decrease in mass on TG curve in the temperature range of 400–740 $^{\circ}$ C due to release of CO₂ from the sample. The DSC curve in this temperature range (Fig. 5, 0 rpm) shows a broad endothermic effect with three distinct peaks at 575, 675 and 725 $^{\circ}$ C. This indicates a three-stage lithium ferrite synthesis reaction. The first two stages in the

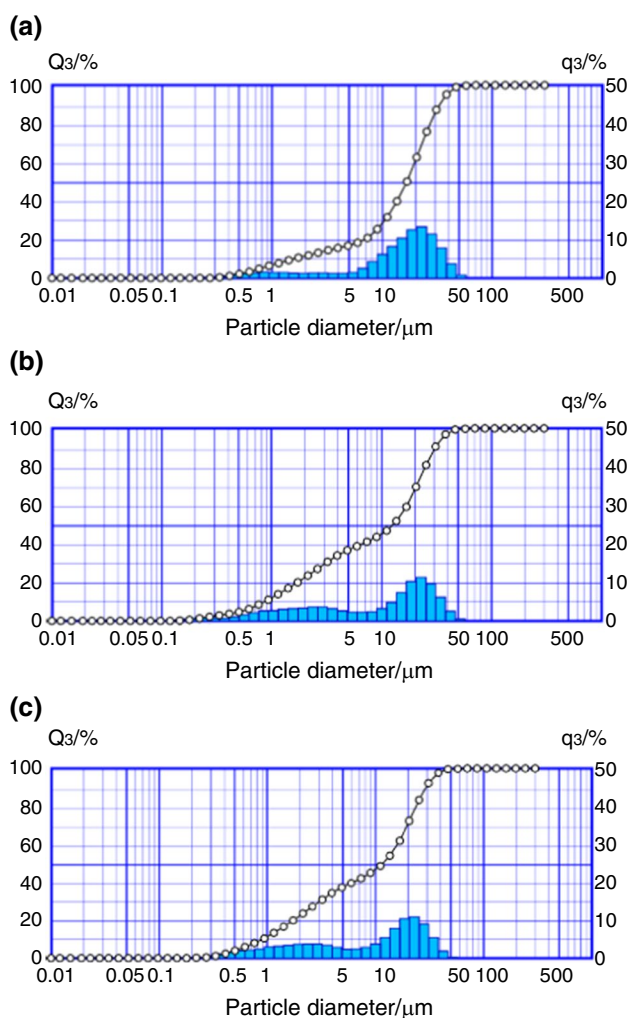


Fig. 3 Particle size distribution of non-activated (a), activated at 1290 rpm (b) and 2220 rpm (c) powder mixtures

Table 1 Particle size distribution from laser diffraction analysis

Powders mixture	$D_{10}/\mu\text{m}$	$D_{50}/\mu\text{m}$	$D_{90}/\mu\text{m}$	Reference
α -Fe ₂ O ₃	0.5	12.1	25.6	[28]
Li ₂ CO ₃	5.7	47.2	212.9	
Non-activated	1.6	16.7	33.2	Present work
Activated at 1290 rpm	0.9	12.6	30.6	
Activated at 2220 rpm	0.9	11.6	29.3	

temperature range of 400–700 $^{\circ}$ C are associated with the formation of the Li_{0.5}Fe_{2.5}O₄ lithium ferrite phase and the LiFeO₂ transition phase, which is formed at a high rate at the beginning of the reaction. It should be noted that, in general, the solid-phase reaction of ferrite formation proceeds in parallel processes:

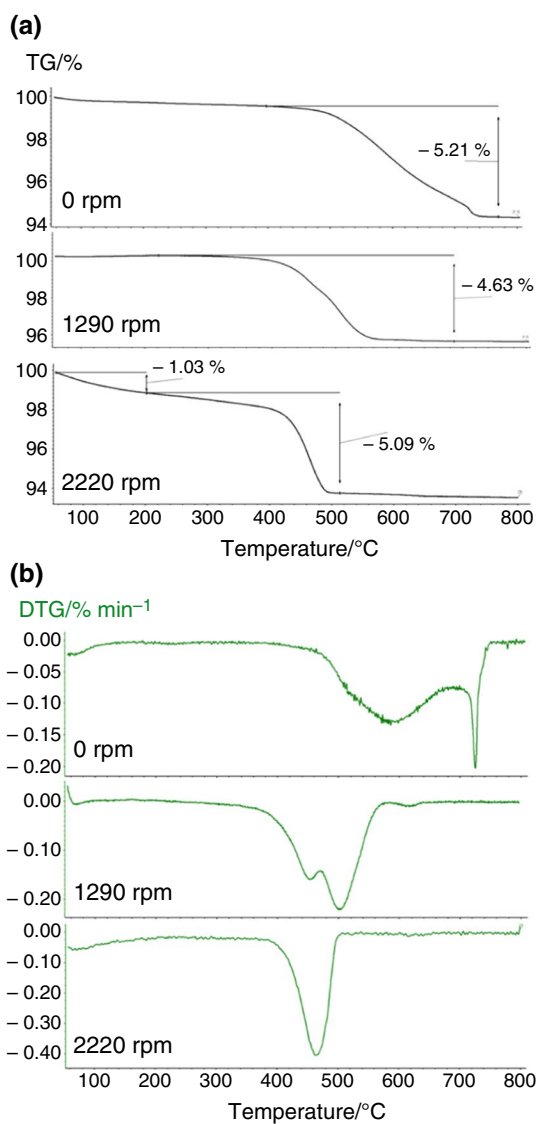
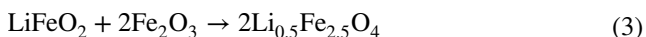
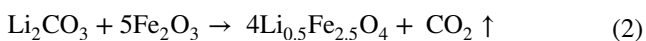
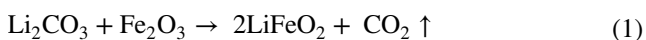


Fig. 4 TG (a) and DTG (b) curves for Fe₂O₃/Li₂CO₃ samples



The results obtained in [34] show that the rival of the considered reactions causes a complex DSC effect. In this case, LiFeO₂ is formed efficiently at up to 600 °C. However, at temperatures exceeding this value, the rate of Li_{0.5}Fe_{2.5}O₄ synthesis sharply increases, and the amount of LiFeO₂ starts to decrease.

A single pronounced peak on the DSC curve at 725 °C in Fig. 5 for 0 rpm sample is associated with melting of lithium

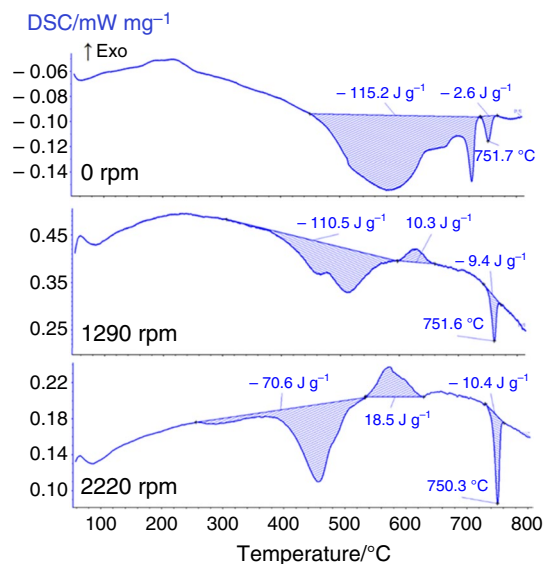


Fig. 5 DSC curves for Fe₂O₃/Li₂CO₃ samples

carbonate residues, which did not react with iron oxide, and lithium carbonate intense interaction in the reaction that affects the rate of the mass loss at this temperature. The total mass loss of 5.21% is close to the calculated value (5.05%) corresponding to the total release of CO₂ upon complete decomposition of lithium carbonate in Eq. (2).

The temperature point of the S_{α-β} peak on the DSC curve at 751.7 °C in Fig. 5 associated with the α → β transition in the Li_{0.5}Fe_{2.5}O₄ phase does not depend on the heating rate and density of the powder mixture. However, as noted above, the peak area depends on the amount of ferrite formed. Taking the previously determined value for this transition equal to 13 J g⁻¹ at 100 mass% Li_{0.5}Fe_{2.5}O₄ [30], the obtained S_{α-β} of 2.6 J g⁻¹ on the DSC curve for the non-activated sample is found to correspond to the formation of 20 mass% lithium ferrite upon reaching 751 °C. In this regard, the remaining 80 mass% is assumed to consist of LiFeO₂ and Fe₂O₃.

The result of the thermal analysis performed using a magnetic field at the cooling stage for non-activated sample is presented in Fig. 6. A sharp mass change indicated by the TG(M) curve (Fig. 6a) is due to the sample interaction with an external magnetic field. The temperature for the change corresponds to the Curie temperature of the magnetic phase in the sample. The resulting value of 633 °C (Fig. 6b) is close to the ferrimagnet-paramagnetic transition temperature for Li_{0.5}Fe_{2.5}O₄ [36, 37]. The obtained value of the mass change also indicates the amount of the magnetic ferrite phase in the sample. With regard to the mass change for pure lithium ferrite equal to 0.41%, which was obtained under similar experimental conditions in [35], the amount of ferrite in the sample is found to be equal to 24 mass%. In contrast to the results

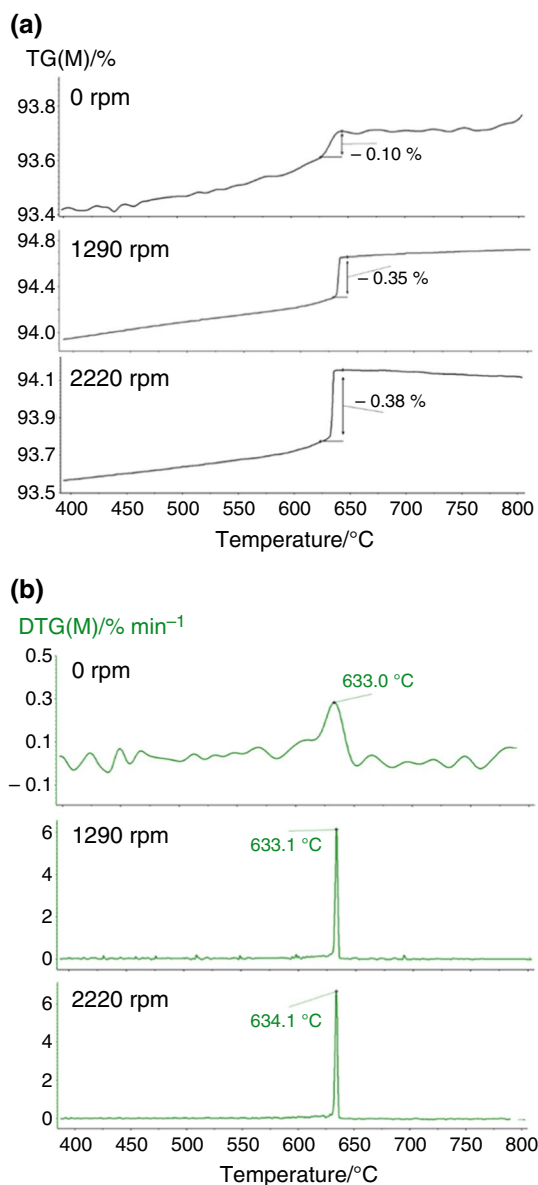


Fig. 6 TG(M) (a) and DTG(M) (b) curves for $\text{Fe}_2\text{O}_3/\text{Li}_2\text{CO}_3$ samples

obtained in heating, higher ferrite content in the sample observed in cooling is associated with the additional formation of ferrite due to heating between the temperature points analyzed.

Figures 4–6 present the results of the thermal analysis for samples mechanically activated at 1290 rpm and 2220 rpm for 120 min. In a powder mixture activated at 1290 rpm, ferrite synthesis begins at 400 °C for samples milled at different times and terminates at 600–700 °C depending on the milling time. Figure 7 shows the dependence of the final reaction temperature (T_r) on the mechanical activation time in more detail. As can be seen, the T_r for the milling time exceeding 30 min is 100 °C lower than that observed in interaction between non-activated reagents. The total mass

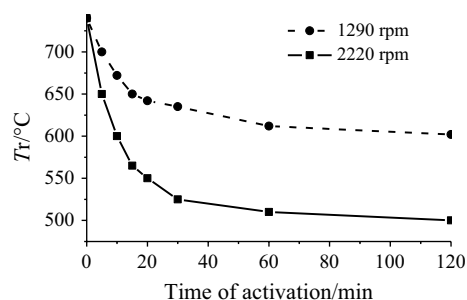


Fig. 7 Final reaction temperature of $\text{Fe}_2\text{O}_3\text{--Li}_2\text{CO}_3$ interaction as a function of milling time

loss in all the samples activated at 1290 rpm corresponds to the calculated CO_2 yield according to Eq. (2).

For such samples, the DSC curve (Fig. 5, 1290 rpm) illustrates a two-stage process with a total enthalpy close to the heat effect observed for non-activated powders. The peak corresponding to this process is not represented on the DSC curve since the reaction terminates before the melting point of lithium carbonate. However, an exothermic peak can be observed at 620 °C. The nature of the process at the given temperature was not clarified in this study. The release of CO_2 in this region can be found only using the mass spectrometric data.

It should be noted that the behavior of the TG/DSC curves for the samples synthesized from powders activated for 30–120 min is very similar. From Fig. 8, the $S_{\alpha-\beta}$ increases as the milling time grows up, which indicates an increase in the amount of the synthesized phase of lithium ferrite. However, at the milling time above 30 min, the content of the ferrite phase in the sample grows very slowly. A similar conclusion can be drawn based on the results of the TG(M) analysis, from which the Δm values obtained at the Curie point are shown in Fig. 9.

For the powder mixture activated at 2220 rpm, the ferrite synthesis reaction starts at 200 °C and terminates at 500–600 °C depending on the milling time (Fig. 4, 2220 rpm). In this case, the mass change observed on

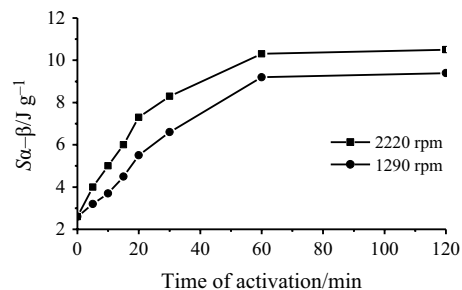


Fig. 8 DSC peak area at the order–disorder transition in the $\text{Li}_{0.5}\text{Fe}_{2.5}\text{O}_4$ ferrite phase as a function of milling time

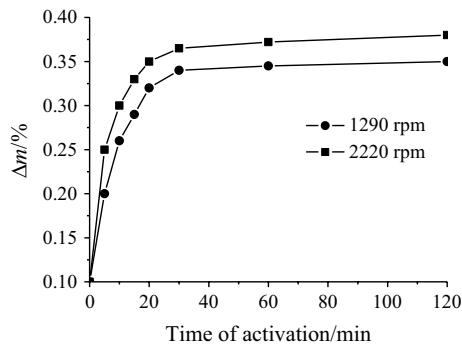


Fig. 9 Mass change at the Curie point from TG(M) analysis as a function of milling time

the TG curve up to 200 °C is associated with the release of water and carbon dioxide molecules adsorbed during mechanical activation or during storage of the powder mixture [23]. The behavior of the DSC curve (Fig. 5, 2220 rpm) for this sample indicates mainly a two-stage process in the reaction of reagent interaction. Moreover, the first stage in the temperature range of 200–400 °C corresponds to a small mass change and insignificant thermal effect associated with it. Comparison of the DSC curves presented in Fig. 5 shows a shift of both reaction stages to the region of lower temperatures as milling energy intensity increases.

As can be seen from Figs. 8 and 9, the patterns of changes in the ferrite phase content during synthesis of the samples from a powder mixture activated at 1290 rpm and 2220 rpm are similar. The content of the ferrite phase increases strongly with an increase in milling time up to 30 min and then slowly grows with a further increase in the milling time. In addition, the content of the ferrite phase increases with increasing vial rotation speed. Moreover, the data obtained in cooling mode indicate a high content of the magnetic ferrite phase in the samples synthesized from powders milled for 30 min.

The results obtained in [29] showed that the main factors that increase the reactivity of powders during their mechanical activation are a decreased particle size and formation of dense agglomerates, which increase the density of the contact between particles. The results obtained in this study confirm the previously drawn conclusions.

The theoretical calculation of the supplied energy during mechanical activation in order to predict the formation of structural changes is associated with certain difficulties. Bernhardt et al. [38] and Husemann et al. [39] indicated the factors that affect the effectiveness of mechanical action in various mills. For mechanical activation in planetary mills, the supplied energy (in terms of the mass of the milled powder) can be estimated from the following equation:

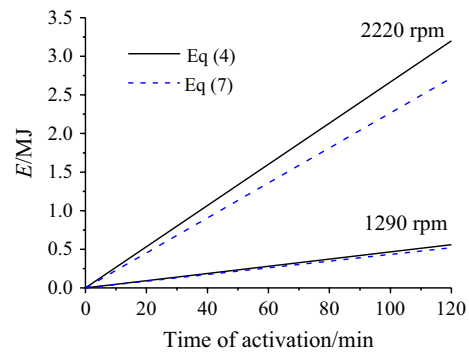


Fig. 10 The total kinetic energy released from the balls to the powder as a function of milling time

$$E = \frac{m_b}{m_p} b \omega D t \quad (4)$$

where m_b and m_p are the mass of the balls and the mass of the powder, respectively; b is the acceleration of the milling material; ω is the rotation speed of vials; D is the diameter of the mill; t —mechanical activation time.

Abdellaoui and Gaffet [40] suggested the equations to estimate the velocity impact (\vec{V}_c) and kinetic energy (E_k in J per hit) transferred from ball to powder during milling:

$$\|\vec{V}_c\|_c^2 = (R)^2 + (r - r_b)^2 \omega^2 \left(1 + \frac{2\omega}{\Omega}\right) \quad (5)$$

$$E_k = \frac{1}{2} m_b \|\vec{V}_c\|_c^2 \quad (6)$$

where R is the distance between the disk center and vial center; Ω and ω are the vial and disc rotation speed in rpm, respectively; m is the ball mass; r and r_b are the vial and ball radius, respectively. The total kinetic energy released from the ball to the powder is

$$E = P t = f E_k t \quad (7)$$

where P is the powder released by the ball to the powder; f is the shock frequency that is associated with the number of collisions per second. Burgio et al. [41] proposed the equations to estimate the kinetic energy in the case of using several balls during milling, wherein the shock frequency is equal to the product of one ball frequency as calculated above and the number of balls corrected by a factor of 1 or less.

The values of the total kinetic energy corresponding to the experimental ball-milling conditions were obtained using Eqs. (4) and (7) and are shown in Fig. 10.

The total kinetic energy values, corresponding to the experimental conditions, were obtained using Eqs. (4) and (7) and are shown in Fig. 10. One can notice that the results

of calculations performed using both proposed models are approximately the same. According to the results, the supplied energy is linearly dependent on the milling time. An increase in the rotation speed of the vials from 1290 to 2220 rpm leads to an increase in the supplied energy by 5–6 times. Thus, it should be expected that milling energy intensity makes a more significant contribution to the change in reactivity than a longer milling time. In addition, it was known that with an increase in the milling time after a certain value, a strong agglomeration of the crushed particles occurs [42–44]. This slows down the further process of particles milling.

Conclusions

The effect of energy intensity (1290 and 2220 rpm) and time (0–120 min) of milling during mechanical activation in a planetary ball mill on the dispersity and reactivity of the α -Fe₂O₃/Li₂CO₃ powder mixture was investigated using laser diffraction analysis, thermogravimetry and differential scanning calorimetry.

It was found that the nature of interaction between the initial powders depends on the mechanical activation mode. The results obtained using laser diffraction showed a reduced average particle size of the powders at increased milling energy intensity.

The results of thermal analysis showed that the temperature range of the initial reagent interaction depends on the time and energy intensity of milling. An increased time and vial rotation speed during mechanical activation shift the final reaction temperature to the region of lower temperatures, and it decreases by 100 °C and 200 °C at 1290 rpm and 2220 rpm milling, respectively. At the same time, temperature at the reaction onset decreases significantly when the initial powders are activated at high energy intensity. Thermal effects established by calorimetry revealed three stages of the reaction of ferrite formation from non-activated powders. In contrast, the reaction is characterized by a two-stage process during synthesis of ferrite from powders activated under all modes.

A changed course of the synthesis reaction is followed by changes in the amount of synthesized lithium ferrite. Thus, an increased time and energy intensity of milling increase the ferrite content during thermal analysis, which indicates an increased reactivity of the activated reagents. However, an increased vial rotation speed during milling makes a more significant contribution to changes in the reactivity of powders than a longer milling time.

Acknowledgements This work was supported by the Ministry of Science and Higher Education of the Russian Federation as part of the

Science program (project FSWW-2020-0008). The experimental part was supported by Tomsk Polytechnic University development program.

References

1. Widatallah HM, Johnson C, Berry FJ. The influence of ball milling and subsequent calcination on the formation of LiFeO₂. *J Mater Sci.* 2002;37:4621–5.
2. Berbenni V, Bruni G, Milanese C, Girella A, Marini A. Synthesis and characterization of LaFeO₃ powders prepared by a mixed mechanical/thermal processing route. *J Therm Anal Calorim.* 2018;133:413–9. <https://doi.org/10.1007/s10973-017-6878-z>.
3. Mazen SA, Abu-Elsaad NI. Structural, magnetic and electrical properties of the lithium ferrite obtained by ball milling and heat treatment. *Appl Nanosci.* 2015;5:105–14. <https://doi.org/10.1007/s13204-014-0297-2>.
4. Nazir MA, Ul-Islam M, Ali I, Ali H, Ahmad B, Ramay SM, Nadeem R, Ehsan MF, Ashiq MN. Structural, electrical and dielectric properties of multiferroic-spinel ferrite composites. *J Electron Mater.* 2016;45:1065–72. <https://doi.org/10.1007/s11664-015-4286-3>.
5. Guo HS, Li LZ, Wang R, Xiong Z, Yan YL, Zhong ZC, Chang X. Cd-substituted NiZnCo ferrite with high dielectric constant and low coercivity for high-frequency electronic devices. *Ceram Int.* 2021. <https://doi.org/10.1016/j.ceramint.2021.10.141>.
6. Amin AMM, Soliman YMM, El-Dek SI, Ahmed YMZ, Zaki AH. Valorization of industrial iron and zinc sludges for the synthesis of ZnFe₂O₄ ceramics. *J Magn Magn Mater.* 2022;544: 168681. <https://doi.org/10.1016/j.jmmm.2021.168681>.
7. Rana G, Dhiman P, Kumar A, Vo DVN, Sharma G, Sharma Sh, Naushad M. Recent advances on nickel nano-ferrite: a review on processing techniques, properties and diverse applications. *Chem Eng Res Des.* 2021;175:182–208. <https://doi.org/10.1016/j.cherd.2021.08.040>.
8. Chang J, Zhan T, Peng X, Li J, Yang Y, Xu J, Hong B, Jin D, Jin H, Wang X, Ge H. Improved permeability and core loss of amorphous FeSiB/Ni–Zn ferrite soft magnetic composites prepared in an external magnetic field. *J Alloys Compd.* 2021;886: 161335. <https://doi.org/10.1016/j.jallcom.2021.161335>.
9. Wang R, Zhou T, Zhong Z. Low-temperature processing of LiZn-based ferrite ceramics by co-doping of V₂O₅ and Sb₂O₃: composition, microstructure and magnetic properties. *J Mater Sci Technol.* 2022;99:1–8. <https://doi.org/10.1016/j.jmst.2021.06.003>.
10. Sarkar K, Mondal R, Dey S, Majumder S, Kumar S. Presence of mixed magnetic phase in mechanically milled Co_{0.5}Zn_{0.5}Fe₂O₄: a study on structural, magnetic and hyperfine properties. *J Magn Magn Mater.* 2019;487:165303. <https://doi.org/10.1016/j.jmmm.2019.165303>.
11. Thang PD, Co ND, Anh HT, Dung DD, Dong QV, Manh TV, Lee BW, Phan TL, Dang NT, Khan DT. Structural, magnetic and electric properties of Sr_{0.95}Y_{0.05}Fe_{12-x}Zr_xO₁₉ (x = 0–2) M-type hexaferrites. *J Magn Magn Mater.* 2022;544:168648. <https://doi.org/10.1016/j.jmmm.2021.168648>.
12. Jianfeng C, Yingli L, Qisheng Y. Computational and experimental study on cation distribution of Cobalt substituted barium hexaferrites BaFe_{12-x}Co_xO₁₉ (x = 0, 0.3, 0.6, 0.9) for circulator applications. *J Alloys Compd.* 2022;891:161917. <https://doi.org/10.1016/j.jallcom.2021.161917>.
13. Gupta S, Sathe VG, Suresh KG, Siruguri V. Evidence for cluster spin-glass like phase with longitudinal conical magnetic structure in Ga doped M-type barium hexaferrite BaFe₁₀Ga₂O₁₉. *J Magn Magn Mater.* 2021;540: 168483. <https://doi.org/10.1016/j.jmmm.2021.168483>.

14. Zhou S, Yang Y, Lei R-Y, Zhou J-P, Chen X-M. The effects of indium doping on the electrical, magnetic, and magnetodielectric properties of M-type strontium hexaferrites. *J Magn Magn Mater*. 2021;539:168333. <https://doi.org/10.1016/j.jmmm.2021.168333>.
15. Dong B, Yang H, Yu L, Cui Y, Jin W, Feng S. The synthesis and the magnetic properties of $\text{Sm}_x\text{BiY}_{2-x}\text{Fe}_5\text{O}_{12}$ nanoparticles. *J Mater Sci*. 2007;42:5003–6. <https://doi.org/10.1007/s10853-006-1311-8>.
16. Zanatta SC, Cotica LF, Paesano A, Medeiros SN, Cunha JBM, Hallouche B. Mechanochemical synthesis of gadolinium iron garnet. *J Am Ceram Soc*. 2005;88:3316–21.
17. Nili-Ahmadabadi M, Sarraf-Mamoory R, Yourdkhani A, Diaconu A, Rotaru A. Magnetic and electrical properties of $\text{Mg}_{1-x}\text{Co}_x\text{Fe}_2\text{O}_4$ ($x = 0-0.15$) ceramics prepared by the solid-state method. *J Eur Ceram Soc*. 2021. <https://doi.org/10.1016/j.jeurceramsoc.2021.10.046>.
18. Mazen SA, Elsayed HM, Abu-Elsaad NI. Effect of divalent metal ions substitution on structural and magnetic properties. *Mater Chem Phys*. 2020;256:123676. <https://doi.org/10.1016/j.matchemphys.2020.123676>.
19. Onderko F, Birčáková Z, Dobák S, Kollár P, Tkáč M, Fáberová M, Fúzer J, Bures R, Szabó J, Zelenáková A. Magnetic properties of soft magnetic $\text{Fe@SiO}_2/\text{ferrite}$ composites prepared by wet/dry method. *J Magn Magn Mater*. 2022;543: 168640. <https://doi.org/10.1016/j.jmmm.2021.168640>.
20. Phan TL, Nguyen HH, Jeong WH, Idczak R, Tran VH, Yang DS, Lee BW. X-ray absorption and Mössbauer spectra, and microwave absorption of (Co, Mn)-doped $\text{SrFe}_{12}\text{O}_{19}$ hexaferrites. *Curr Appl Phys*. 2021;29:114–21. <https://doi.org/10.1016/j.cap.2021.07.002>.
21. Thang PD, Tiep NH, Ho TA, Co ND, Hong NTM, Dong QV, Lee BW, Phan TL, Dang NT, Khan DT, Yang DS. Electronic structure and multiferroic properties of (Y, Mn)-doped barium hexaferrite compounds. *J Alloys Compd*. 2021;867: 158794. <https://doi.org/10.1016/j.jallcom.2021.158794>.
22. Lysenko EN, Surzhikov AP, Nikolaev EV, Vlasov VA. Thermal analysis study of LiFeO_2 formation from $\text{Li}_2\text{CO}_3\text{-Fe}_2\text{O}_3$ mechanically activated reagents. *J Therm Anal Calorim*. 2018;134:81–7. <https://doi.org/10.1007/s10973-018-7113-2>.
23. Lysenko EN, Surzhikov AP, Vlasov VA, Malyshev AV, Nikolaev EV. Thermal analysis study of solid-phase synthesis of zinc- and titanium-substituted lithium ferrites from mechanically activated reagents. *J Therm Anal Calorim*. 2015;122:1347–53. <https://doi.org/10.1007/s10973-015-4849-9>.
24. Hajalilou A, Kianvash A, Lavvafi H, Shameli K. Nanostructured soft magnetic materials synthesized via mechanical alloying: a review. *J Mater Sci Mater Electron*. 2018;29:1690–717. <https://doi.org/10.1007/s10854-017-8082-0>.
25. Hajalilou A, Hashim M, Ebrahimi-Kahrizangi R, Mohamed Kamari H, Kanagesan S. Parametric optimization of NiFe_2O_4 nanoparticles synthesized by mechanical alloying. *Mater Sci Pol*. 2014;32(2):281–91. <https://doi.org/10.2478/s13536-013-0173-x>.
26. Berbenni V, Marini A, Matteazzi P, Ricceri R, Welham NJ. Solid-state formation of lithium ferrites from mechanically activated $\text{Li}_2\text{CO}_3\text{-Fe}_2\text{O}_3$ mixtures. *J Eur Ceram Soc*. 2003;23:527–36. [https://doi.org/10.1016/S0955-2219\(02\)00150-4](https://doi.org/10.1016/S0955-2219(02)00150-4).
27. Widatallah HM, Berry FJ. The influence of mechanical milling and subsequent calcination on the formation of lithium ferrites. *J Solid State Chem*. 2002;164:230–6. <https://doi.org/10.1006/jssc.2001.9466>.
28. Kavanlooe M, Hashemi B, Maleki-Ghaleh H, Kavanlooe J. Effect of annealing on phase evolution, microstructure, and magnetic properties of nanocrystalline ball-milled LiZnTi ferrite. *J Electron Mater*. 2012;41:3082–6. <https://doi.org/10.1007/s11664-012-2235-y>.
29. Surzhikov AP, Lysenko EN, Vlasov VA, Nikolaev EV. Microstructure and reactivity of $\text{Fe}_2\text{O}_3\text{-Li}_2\text{CO}_3\text{-ZnO}$ ferrite system ball-milled in a planetary mill. *Thermochim Acta*. 2018;664:100–7. <https://doi.org/10.1016/j.tca.2018.04.015>.
30. Lysenko EN, Nikolaev EV, Surzhikov AP, Nikolaeva SA, Plotnikova IV. The influence of reagents ball milling on the lithium ferrite formation. *J Therm Anal Calorim*. 2019;138:2005–13. <https://doi.org/10.1007/s10973-019-08334-1>.
31. Shinde BL, Mandle UM, Pachpinde AM, Lohar KS. Synthesis and characterization of Al^{3+} substituted Ni–Cu–Zn nanoferrites. *J Therm Anal Calorim*. 2021. <https://doi.org/10.1007/s10973-021-10719-0>.
32. Wang G, Min X, Peng N, Wang Zh. The isothermal kinetics of zinc ferrite reduction with carbon monoxide. *J Therm Anal Calorim*. 2021;146:2253–60. <https://doi.org/10.1007/s10973-020-10542-z>.
33. Dessai PPG, Verenkar VMS. Synthesis and characterization of $\text{Ni}_{0.7-x}\text{Mn}_x\text{Zn}_{0.3}\text{Fe}_2(\text{C}_4\text{H}_2\text{O}_4)_3 \cdot 6\text{N}_2\text{H}_4$ ($x = 0.1-0.6$): a precursor for the synthesis of nickel–manganese–zinc ferrites. *J Therm Anal Calorim*. 2020;142:1399–411. <https://doi.org/10.1007/s10973-020-09485-2>.
34. Lysenko EN, Nikolaev EV, Vasendina EA. Investigation of heating rate effect on solid-phase interaction in $\text{Li}_2\text{CO}_3\text{-Fe}_2\text{O}_3$ reaction mixture. *IOP Conf Ser Mater Sci Eng*. 2015;81: 012104. <https://doi.org/10.1088/1757-899X/81/1/012104>.
35. Lysenko EN, Surzhikov AP, Astafyev AL. Thermomagneto-metric analysis of lithium ferrites. *J Therm Anal Calorim*. 2019;136:441–5. <https://doi.org/10.1007/s10973-018-7678-9>.
36. Smit J, Wijn HPJ. Ferrites, physical properties of ferrimagnetic oxides in relation to their technical applications. Amsterdam: Philips Technical Library; 1959.
37. White GO, Patton CE. Magnetic properties of lithium ferrite microwave materials. *Magn Magn Mater*. 1978;9:299–317. [https://doi.org/10.1016/0304-8853\(78\)90085-9](https://doi.org/10.1016/0304-8853(78)90085-9).
38. Bernhardt C, Heegn H. Mechanical activation in fine grinding mills [Zur mechanischen Aktivierung in Feinzerkleinerungsmaschinen]. *Dechema Monogr*. 1975;79:213–25.
39. Husemann K, Bernhardt C, Heegn H. Feinmahlung und mechanische aktivierung von eisenpulver. *Powder Technol*. 1976;14:41–9.
40. Abdellaoui M, Gaffet E. A mathematical and experimental dynamical phase diagram for ball-milled $\text{Ni}_{10}\text{Zr}_7$. *J Alloys Compd*. 1994;209:351–61. [https://doi.org/10.1016/0925-8388\(94\)91124-X](https://doi.org/10.1016/0925-8388(94)91124-X).
41. Burgio N, Iasonna A, Magini M, Martelli S, Padella F. Mechanical alloying of the Fe–Zr system. Correlation between input energy and end products. *Nuovo Cimento D*. 1991;13(4):459–76. <https://doi.org/10.1007/BF02452130>.
42. Boldyrev VV. Mechanochemistry and mechanical activation of solids. *Russ Chem Rev*. 2006;75:177–89.
43. Schönert K. Physical and technical aspects of very and micro fine grinding. In: *Proceedings of Second World Congress Particle Technology*. Kyoto: Society of Powder Technology; 1990. p. 257–71.
44. Šepelák V, Bergmann I, Kipp S, Becker KD. Nanocrystalline ferrites prepared by mechanical activation and mechanochemical synthesis. *Z Anorg Allg Chem*. 2005;631:993.

Publisher's Note Springer Nature remains neutral with regard to jurisdictional claims in published maps and institutional affiliations.